Seventh International Conference on CFD in the Minerals and Process Industries
CSIRO, Melbourne, Australia
9-11 December 2009

COMPUTATIONAL SIMULATION OF RED BLOOD CELL MOTION IN MICROVESSEL BIFURCATIONS

Timothy W. SECOMB[1], Jared O. BARBER[2] and Juan M. RESTREPO[3]
[1]Department of Physiology, [2]Program in Applied Mathematics, [3]Department of Mathematics,
University of Arizona, Tucson, AZ 85724, USA

ABSTRACT

A two-dimensional computational model is used to simulate the motion of red blood cells (RBCs) in diverging microvessel bifurcations. The RBC is represented as a set of interconnected viscoelastic elements suspended in a viscous fluid. The equations of equilibrium and fluid motion are solved using a finite-element method. Centre-of-mass trajectories deviate from background flow streamlines due to migration of the cells toward the vessel centre-line upstream of the bifurcation and due to cell obstruction of the flow near the bifurcation. RBCs tend to enter the higher-flow branch, leading to unequal cell fractions in the downstream branches (phase separation). This effect is increased by migration toward the centre-line but decreased by the effects of obstruction. When two closely spaced cells pass through a bifurcation, if the first cell enters the high-flow branch, the second cell tends to enter the low-flow branch. Therefore, phase separation behaviour decreases with increasing cell fraction.

Keywords: erythrocytes, microcirculation, hematocrit, phase separation, Stokes flow

INTRODUCTION

The microvessels, with diameters as small as 4 μm, are the terminal branches of the circulatory system. Blood is a concentrated suspension, containing 40-45% by volume of red blood cells (erythrocytes) suspended in plasma. The mechanical properties of human RBCs have been studied extensively (Skalak, 1976;Hochmuth and Waugh, 1987). The unstressed shape of a normal human RBC is a biconcave disc with a diameter of 8 μm and a thickness of 2 μm. The interior of the cell behaves as a viscous incompressible fluid. The cell membrane consists of a lipid bilayer and a cytoskeleton which consists of a network of protein molecules. The membrane strongly resists area changes, and its elastic modulus of isotropic dilation is ~500 dyn/cm, whereas its modulus of shear deformation is about 0.006 dyn/cm. The lipid molecules that comprise the lipid bilayer can slide past each other relatively easily, but resist being pulled apart. The cell membrane has a relatively small bending modulus, about 1.8×10^{-12} dyn·cm (Evans, 1983). The membrane also possesses a viscous resistance to transient in-plane shear deformations. The viscoelastic behaviour of the membrane in shear can be represented by a Kelvin solid model, in which the total shear stress is represented as the sum of viscous and elastic contributions (Evans and Hochmuth, 1976). The viscous component arises from the fluid-like behaviour of the lipid bilayer, and the elastic component arises from the stretching of the cytoskeleton.

When blood passes through diverging bifurcations in the microcirculation, the fraction of RBCs entering a given daughter branch is generally not equal to the fraction of the total flow entering that branch. This non-uniform partitioning of haematocrit is responsible for the heterogeneous haematocrit distribution that is observed in the microvasculature. In experimental studies (Schmid-Schonbein et al., 1980), blood flow was observed in rabbit ear capillary bifurcations with diameters ~ 5-15 μm. The dependence of the fractions of RBC flux in the two daughter branches on the fractions of bulk blood flux into those branches was determined. The results suggested that the upstream haematocrit distribution significantly influences RBC partitioning at a diverging bifurcation.

Observations (Pries et al., 1989) of arteriolar bifurcations in rat mesentery indicated several parameters that affect the fraction of RBC flux entering a branch: the fraction of bulk blood flux entering that branch, the ratio of the two daughter vessel diameters, the size of the mother vessel, and the upstream haematocrit distribution. A function of those parameters was constructed that gives an estimate of the RBC flux into the two daughter branches of a bifurcation. This function was later refined (Pries and Secomb, 2005).

Here, the motion of RBCs in microvessel bifurcations is examined using a computational model of flexible two-dimensional RBCs (Secomb et al., 2007). Mechanical effects underlying the tendency of RBCs to drift, or migrate, across underlying fluid streamlines in small vessel bifurcations (6-13 μm) are analysed. Effects of particle deformability are examined by comparing the results with those obtained in corresponding simulations using rigid particles. Effects of cell-to-cell interaction are examined by comparing simulations of a cell passing through a bifurcation alone with simulations of two cells passing through a bifurcation at the same time. The results are used to predict RBC partitioning in small vessel bifurcations and its dependence on mother vessel size, ratio of daughter diameters, daughter branching angles, and cell deformability.

MODEL DESCRIPTION

A two-dimensional model is used to describe the motion of one or more RBCs in a surrounding Stokes flow as it moves in a rigid vessel. The constraint of constant cell volume that would apply in the three-dimensional case is represented by an effective internal pressure (Secomb et al., 2007). Nodes are located along the perimeter of the RBC, with an additional internal node, as shown in Fig. 1A. The outer line segments (external elements) are viscoelastic, and represent a planar cross-section of a RBC membrane that possesses shear elasticity, bending elasticity, and in-plane viscosity. The segments connecting the central node to the outer nodes (internal elements) are viscous and are included to represent effects

Copyright © 2009 CSIRO Australia

of viscous resistance to cytoplasmic flow and out-of-plane membrane deformation.

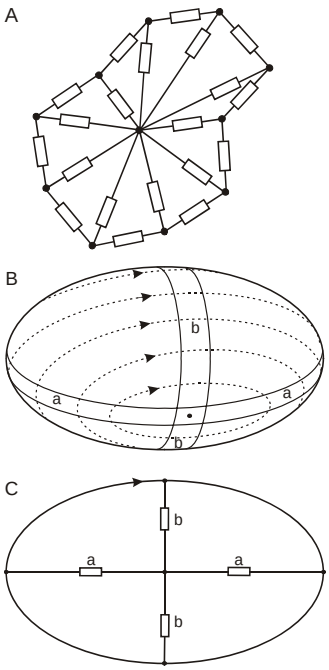

Figure 1. A. Two-dimensional model for RBC. Rectangles represent viscoelastic elements. B, C. Relationship between internal viscous elements and membrane deformation in tank-treading. Bands of membrane (a,b) alternately shorten and elongate during tank-treading.

The outer nodes are numbered from 1 to n and the i^{th} node has coordinates $\boldsymbol{x}_i = (x_i,y_i)$. The central node has coordinates $\boldsymbol{x}_0 = (x_0,y_0)$. An external element and the quantities associated with it are denoted by i when the element's endpoints are (x_i,y_i) and (x_{i+1},y_{i+1}). The i^{th} internal element has as its endpoints (x_0,y_0) and (x_i,y_i).

The average tension in external element i is given by

$$\bar{t}_i = k_t(l_i/l_0 - 1) + \mu_m \frac{1}{l_i}\frac{\mathrm{d}l_i}{\mathrm{d}t}, \tag{1}$$

where l_i is the length of the i^{th} external element, $l_0 = 0.97$ μm is a reference length, $k_t = 0.012$ dyn/cm is the elastic modulus, and $\mu_m = 2\times10^{-4}$ dyn s/cm is the viscosity of the external elements. The bending moment acting on the i^{th} node (x_i,y_i) is

$$m_i = -k_b\alpha_i/l_0. \tag{2}$$

Here $k_b = 9 \times 10^{-12}$ dyn cm is the assumed bending modulus at the nodes and α_i is the angle between two consecutive external elements. The internal elements are assumed to have viscous resistance to changes in length,

$$T_i = \mu'_m \frac{1}{L_i}\frac{\mathrm{d}L_i}{\mathrm{d}t}, \tag{3}$$

where L_i is the length of the i^{th} internal element, $\mu'_m = 1\times10^{-4}$ dyn s/cm is the viscosity of the internal elements (Secomb et al., 2007) and T_i is the tension in internal element i.

The fluid inside of the cell is assumed to exert a constant internal pressure on the membrane,

$$p_{int} = k_p(1 - A/A_{ref}), \tag{4}$$

where A is the area of the cell cross-section, $A_{ref} = 22.2$ μm^2 is a reference area and $k_p = 50$ dyn/cm^2. RBC volume preservation and surface area preservation lead to approximately constant cross-sectional area in three-dimensional RBCs, and a relatively large value of k_p is assumed, to represent that property. A_{ref} and l_0 are chosen so that cells develop non-circular shapes with area A_{ref} and perimeter nl_0.

Balancing the tensions and moments acting at each node with the fluid forces acting on the external elements and balancing all viscous forces at the central node yields a system of $2(n+1)$ linear equations in the nodal velocities $\boldsymbol{u}_i = (u_i,v_i)$ and $\boldsymbol{u}_0 = (u_0,v_0)$. This system includes unknown terms dependent on the surrounding flow.

The plasma is assumed to be a viscous, incompressible fluid governed by the Stokes equations:

$$\nabla\cdot\boldsymbol{u} = 0; \quad \nabla\cdot\boldsymbol{\sigma} = 0; \quad \boldsymbol{\sigma} = \mu(\nabla\boldsymbol{u} + \nabla\boldsymbol{u}^T) - p\boldsymbol{I}. \tag{5}$$

Here p is the pressure, $\boldsymbol{u}$ is the velocity, $\boldsymbol{\sigma}$ is the stress tensor, and $\mu = 10^{-2}$ dyn s/cm^2 is the viscosity. The incompressibility condition is replaced by the equation

$$\nabla^2 p = K\nabla\cdot\boldsymbol{u}. \tag{6}$$

Using the stiffness parameter $K \geq 100$ ensures that $\nabla\cdot\boldsymbol{u} \approx 0$.

Fig. 2 shows an example of an assumed vessel bifurcation geometry. At the entrance to the mother vessel, constant pressure and Neumann conditions for $\boldsymbol{u}$ are specified. At exits of the daughter branches, the gradients of p and the values of $\boldsymbol{u}$ are prescribed, corresponding to Poiseuille flow with the specified flow rates. The fraction of bulk blood flow into daughter branch 1, $\Psi_1 = Q_1/Q_0$, is held constant throughout a given simulation as the effect on flow rate of a RBC blocking a daughter vessel is assumed negligible. The flow resistance created by a single cell in the daughter branch is small compared to the total resistance of the vessel downstream of the bifurcation. On the vessel wall, Neumann conditions for p and no-slip conditions for $\boldsymbol{u}$ are imposed.

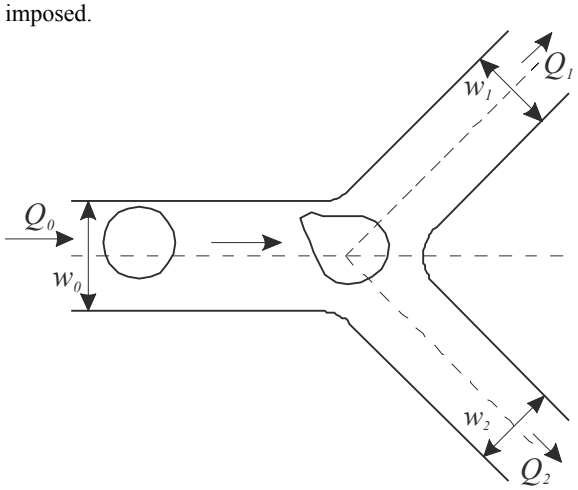

Figure 2. Example of bifurcation geometry considered.

A particle path is represented by the trajectory of its centre of mass, referred to as a particle streamline. For a given vessel geometry and Ψ_1, a separating particle streamline, starting at $y_0 = y_c(\Psi_1)$, separates particle streamlines that enter branch 1 from those that enter branch 2. The separating streamline of the underlying flow is also defined for each flow fraction. The RBC flux into branch 1, as a fraction of the total RBC flux, is given by

Copyright © 2009 CSIRO Australia

$$\Phi_1(\Psi_1) = \frac{\int_{y_c(\Psi_1)}^{y_t} s(y)u_d(y)dy}{\int_{y_b}^{y_t} s(y)u_d(y)dy}. \quad (7)$$

Here $s(y)$ is the density distribution of cell centres as they pass $x = x_0$, assumed to be constant and $u_d(y)$ is the horizontal velocity distribution of the cell centres at x_0.

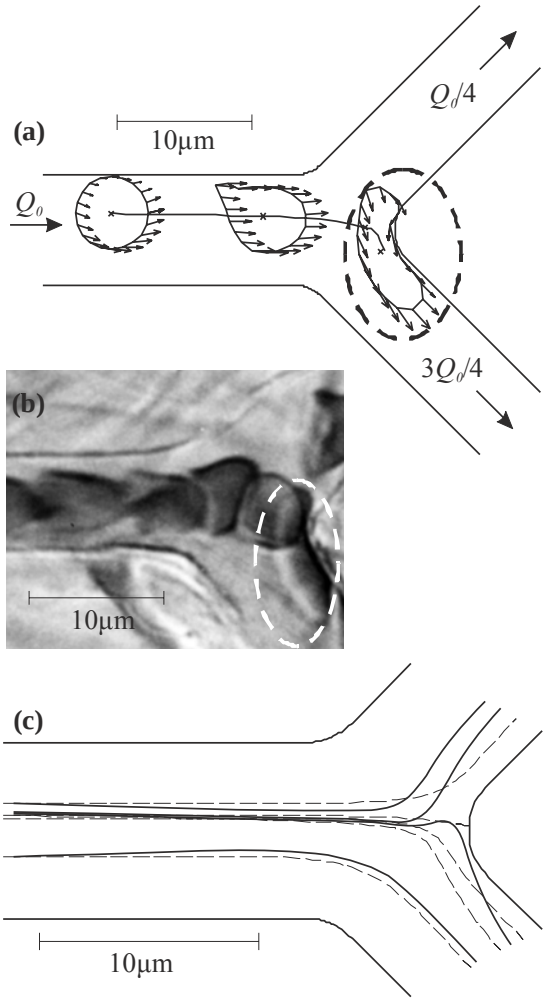

Figure 3. (a) Example of centre-of-mass trajectory, computed cell shapes and individual nodal velocities (arrows) (Barber et al., 2008). Here Q_0 = 8 μm^2/ms, w_0 = 8 μm and Ψ_1 = 3/8. Cell shapes are shown at t = 0, 10, and 30 ms. Dashed ellipse indicates cell in sandbag-like shape, adjacent to the flow divider. (b) Photomicrograph of RBCs in a capillary bifurcation in the rat mesentery (Pries and Secomb, 2008). Scale is as in (a). One cell (indicated by dashed ellipse) is deformed into a sandbag-like shape, corresponding to the computed shape in (a). (c) Computed cell (solid) and underlying fluid (dashed) streamlines for the same geometry and Ψ_1 = ¼. The dashed line that intersects the far wall of the bifurcation is the separating fluid streamline.

RESULTS AND DISCUSSION

Fig. 3(a) shows an example of predicted cell shapes in a symmetric bifurcation. The initially circular cell is deformed into an asymmetric shape similar to observed shapes in capillaries (Secomb et al., 2007). On reaching the flow divider between the two branches, the cell assumes a sandbag-like shape straddling the flow divider. Similar shapes are observed in vivo (Fig. 3(b)). In Fig. 3(c), particle streamlines (solid) are compared with fluid streamlines of the underlying flow field (dashed). Particle streamlines deviate substantially from the corresponding streamlines of the underlying flow. For example, consider the particle streamline closest to the upper boundary in Figure 3(c). As the cell approaches the bifurcation, it migrates away from the wall towards the centreline. Such migration is a characteristic feature of red blood cell motion in capillaries (Secomb et al., 2007). However, after the cell enters and partially obstructs the bifurcation region, it moves in the opposite direction relative to the fluid streamline. These two types of motion can affect the branch that the cell ultimately enters.

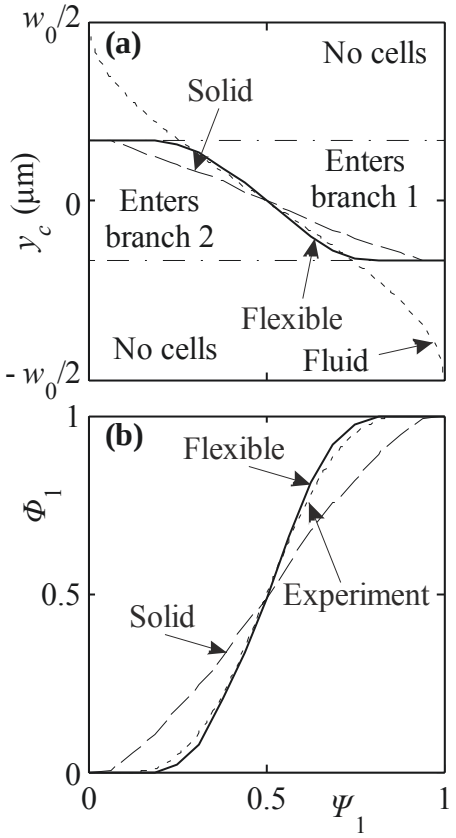

Figure 4. (a) Dependence of position of separating particle streamline on flow fraction entering branch 1. (b) Resulting dependence of red blood cell fraction entering branch 1 on flow fraction entering branch 1.

Results for this bifurcation are summarized in Figure 4. If the flow fraction entering branch 1 is less than a minimum value, no red blood cells enter that branch. This flow fraction corresponds approximately to the condition that the separating fluid streamline of the background flow coincides with the position of a cell centre when it is as close as possible to the wall. For flow fractions in branch 1 larger than this, the separating streamline for the particles (solid curve in upper panel) corresponds closely to the separating streamline of the background flow (dashed line). However, it should be noted that this occurs despite the occurrence of significant particle migration across streamlines. In this example, the two opposite tendencies mentioned in the previous paragraph approximately cancel each other.

Figure 4 also includes results of simulations for the motion of rigid circular particles with approximately the

Copyright © 2009 CSIRO Australia

same area as the flexible particles. Figure 4(b) shows the resulting dependence of red cell fraction on flow fraction entering branch 1. The dashed curve shows corresponding results from the experimentally based empirical formulas (Pries et al., 1989;Pries and Secomb, 2005), indicating close agreement with the result for flexible particles. However, rigid particles showed more uniform haematocrit partitioning, with Φ_1 more nearly proportional to Ψ_1.

In further simulations, the motion of two interacting cells was considered. In this case, a three-dimensional space of initial configurations can be defined for a given geometry and flow partition, in which the transverse positions of the two cells and the time difference between their entries into the flow domain are variables. Time lags of up to 20 ms were considered, corresponding to spatial separations ranging from about 6 μm to 20 μm.

In the majority of the cases within this range, the branch entered by a given cell was not altered by interactions with the other cell. However, several types of interactions were identified leading to a change in branch. For the flow split of $\Psi_1 = 3/8$, a 'trade-off' interaction occurred in about 13% of cases. In such an interaction, the second cell entered the opposite branch to the first cell, although it would have entered the same branch in the absence of interaction. This phenomenon can be understood by considering the configuration shown in Figure 5. A control volume is defined with the separating streamline of the underlying flow as one of the boundaries, as indicated. As the front cell is drawn into the lower branch, a balancing upward component of velocity is generated in the upstream region, which tends to draw the second cell into the upper branch.

Other types of interactions were identified in which the presence of one cell affected the branch entered by the other cell. In the 'herding' effect, the trajectory of the leading cell is affected by the presence of the trailing cell, such that both cells enter the same branch. In the 'following' effect, the front cell influences the branch entered by the rear cell, again causing both to enter the same branch. However, these other interactions occur in less than 2.5% of all cases considered. The net result of all these interactions was that two-cell interactions led to more uniform distribution of haematocrit between the two branches, as observed experimentally (Pries et al., 1989).

CONCLUSION

A two-dimensional model has been developed to predict shapes and trajectories of individual RBCs flowing in capillary bifurcations. The model predicts significant migration of RBCs across streamlines of the underlying flow. Two distinct mechanisms of migration were identified: migration of the cells toward the vessel centre-line upstream of the bifurcation, and migration into a low-flow branch due to obstruction of that branch by the cell in the neighbourhood of the bifurcation. Effects of cell-to-cell interactions were simulated. When two closely spaced cells pass through a bifurcation, the first cell, by entering the high-flow branch, increases the tendency of the second cell to enter the low-flow branch. Therefore, phase separation behaviour is predicted to decrease with increasing cell fraction. Model predictions in are good agreement with experimental observations of haematocrit partition in diverging microvessel bifurcations.

Supported by NIH Grant HL034555.

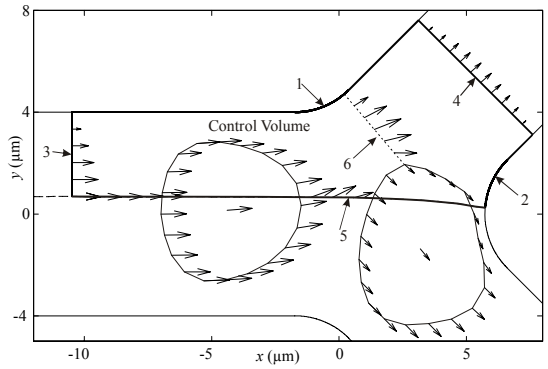

Figure 5. Schematic explanation of the 'trade-off' effect. No fluid flux occurs across lines 1 and 2, which correspond to the vessel walls. The fluid fluxes across lines 3 and 4 must sum to zero, if they are sufficiently far from the cells. Therefore, no net fluid flux occurs across line 5, the background separating fluid streamline. The downward fluid flux across line 5 generated by the leading cell as it enters the lower branch must generate an upward velocity in the upstream region, which affects the trajectory of the trailing cell.

REFERENCES

BARBER, J.O., ALBERDING, J.P., RESTREPO, J.M. and SECOMB, T.W. (2008), "Simulated two-dimensional red blood cell motion, deformation, and partitioning in microvessel bifurcations", *Ann. Biomed. Eng* **36**, 1690-1698.

EVANS, E.A. (1983), "Bending elastic modulus of red blood cell membrane derived from buckling instability in micropipet aspiration tests", *Biophys. J.* **43**, 27-30.

EVANS, E.A. and HOCHMUTH, R.M. (1976), "Membrane viscoelasticity", *Biophys. J.* **16**, 1-11.

HOCHMUTH, R.M. and WAUGH, R.E. (1987), "Erythrocyte membrane elasticity and viscosity", *Annu. Rev. Physiol* **49**, 209-219.

PRIES, A.R., LEY, K., CLAASSEN, M. and GAEHTGENS, P. (1989), "Red cell distribution at microvascular bifurcations", *Microvasc. Res.* **38**, 81-101.

PRIES, A.R. and SECOMB, T.W. (2005), "Microvascular blood viscosity in vivo and the endothelial surface layer", *Am. J. Physiol Heart Circ. Physiol* **289**, H2657-H2664.

PRIES, A.R. and SECOMB, T.W. (2008), "Blood Flow in Microvascular Networks". *In* Handbook of Physiology: Microcirculation. Second Edition. R.F.Tuma, W.N.Duran, and K.Ley, editors. Academic Press, San Diego. 3-36.

SCHMID-SCHONBEIN, G.W., SKALAK, R., USAMI, S. and CHIEN, S. (1980), "Cell distribution in capillary networks", *Microvasc. Res.* **19**, 18-44.

SECOMB, T.W., STYP-REKOWSKA, B. and PRIES, A.R. (2007), "Two-dimensional simulation of red blood cell deformation and lateral migration in microvessels", *Ann. Biomed. Eng* **35**, 755-765.

SKALAK, R. (1976), "Rheology of red blood cell membrane". *In* Microcirculation, Vol. I. J.Grayson and W.Zingg, editors. New York. 53-70.

Copyright © 2009 CSIRO Australia